The Astrophysical Journal, 799:111 (9pp), 2015 January 20 doi:10.1088/0004-637X/799/1/111

ESTIMATION OF THE RELEASE TIME OF SOLAR ENERGETIC PARTICLES NEAR THE SUN

Yang Wang and Gang Qin
State Key Laboratory of Space Weather, Center for Space Science and Applied Research, Chinese Academy of Sciences,
Beijing 100190, China; ywang@spaceweather.ac.cn, gqin@spaceweather.ac.cn
Received 2013 November 28; accepted 2014 November 18; published 2015 January 20

ABSTRACT

This paper investigates the onset time of solar energetic particle (SEP) events with numerical simulations and analyzes the accuracy of the velocity dispersion analysis (VDA) method. Using a three-dimensional focused transport model, we calculate the fluxes of protons observed in the ecliptic at 1 AU in the energy range between 10 MeV and 80 MeV. In particular, three models are used to describe different SEP sources produced by flare or coronal shock, and the effects of particle perpendicular diffusion in the interplanetary space are also studied. We have the following findings. When the observer is disconnected from the source, the effects of perpendicular diffusion in the interplanetary space and particles propagating in the solar atmosphere have a significant influence on the VDA results. As a result, although the VDA method is valid with impulsive source duration, low background, and weak scattering in the interplanetary space or fast diffusion in the solar atmosphere, the method is not valid with gradual source duration, high background, or strong scattering.

Key words: Sun: activity – Sun: coronal mass ejections (CMEs) – Sun: flare – Sun: magnetic fields – Sun: particle emission

1. INTRODUCTION

Solar energetic particles (SEPs) were first reported by Forbush (1946). Because coronal mass ejection (CME) was not discovered at that time, SEPs were assumed to be accelerated by solar flares. If this holds true, it is reasonable to assume that the size of the SEPs source is close to that of the flare. However, some SEP events could be simultaneously observed by multiple spacecraft with a very wide spatial distribution that could be much wider than the size of the flare. In order to interpret this phenomenon, two scenarios were proposed: (1) particles can cross magnetic field lines in the interplanetary space with perpendicular diffusion (McKibben 1972; Dresing et al. 2012, 2014), and (2) particles can propagate in the solar atmosphere (Wibberenz et al. 1989; Dresing et al. 2014). However, the SEP community later realized that CMEs are important for particle acceleration, especially in large SEP events (Mason et al. 1984; Gosling 1993; Zank et al. 2000; Li et al. 2003). As a result, besides the former two scenarios, a third one was proposed: the wide spread of SEPs can be explained by SEPs being accelerated by large-scale shocks. However, large SEP events are usually associated with both flares and CMEs, so the role of flares and shock in the acceleration process of SEPs is still being debated. For the historical development of the studies on the source of SEPs, please refer to the review articles by Reames (1999) and Reames (2013).

Because of the effects of particle transport, it is difficult to distinguish between the signatures of different accelerators in SEP fluxes at 1 AU. However, SEP fluxes observed in the interplanetary space show a velocity dispersion at the onset time. The velocity dispersion analysis (VDA) method has been used widely to investigate SEP acceleration and transport processes (Krucker et al. 1999; Krucker & Lin 2000; Kahler & Ragot 2006; Reames 2009; Tan et al. 2012; Li et al. 2013; Ding et al. 2014). This method assumes that the first-arriving particles move along the magnetic field lines, and the path length traveled by particles between the source and observer is independent of energy. With these assumptions, the SEP release time near the Sun and the interplanetary path length can be determined by using the onset times of different energy particles. In addition, to compare the SEP release time with the electromagnetic signature of the SEP source, the SEP source can be identified.

It has been known for a long time that when an observer is far from the magnetic connection point of the source on the Sun, the onset time of the SEP flux shows a delay (Van Hollebeke et al. 1975; Ma Sung & Earl 1978). This would lead to changes in the results of the VDA method. Krucker et al. (1999) calculated the release time near the Sun and the path length in the interplanetary space of SEPs with 12 short electron events observed by the *Wind* spacecraft. The result of the VDA method indicates two kinds of electron events. In the first kind of event, the electron release time is extremely close to the onset of a radio type III burst when the observer is connected to the flare. In the second kind of event, the electrons are released much later (e.g., half an hour) than the onset of the type III burst when the observer is disconnected from the flare. Huttunen-Heikinmaa et al. (2005) studied the release time of MeV/n protons and heliums observed by *Solar and Heliospheric Observatory* (*SOHO*)/ERNE. They found that the delay in SEP release time derived from the VDA method is related to the poor magnetic connection between the flare site and the spacecraft. For extremely high-energy particle events, Reames (2009) studied the onset time of ion fluxes in ground-level enhancements. They concluded that the time difference between the solar particle release time and the onset time of the metric type II radio burst increases with the angular distance between the observer's magnetic foot-point and the source increase.

According to different heliographic latitude observations, Zhang et al. (2003) analyzed an SEP event simultaneously observed by the *Ulysses* and *GOES* spacecraft. The *GOES* spacecraft is located in the ecliptic, and the *Ulysses* is located at 62° south. The SEP release time derived from the *GOES* data is consistent with the onset of the soft X-ray flux, and the path length is also close to the Parker spiral. In contrast, the release time derived from the *Ulysses* data is three hours later than the onset of the soft X-ray flux, and the path length is much longer than the Parker spiral. Further studies were done by Dalla et al. (2003a, 2003b), who analyzed nine SEP events observed by

Ulysses at high latitudes, among which eight events are observed at latitudes of more than 60°, and the remaining event is observed at 47°.9 latitude. Dalla et al. (2003a, 2003b) found that the path lengths derived from the *Ulysses* data are 1.06–2.45 times the length of the Parker spiral, and the particle release times are between 100 and 350 minutes later than that derived from the *SOHO* and *Wind* measurements. The delay in particle release time increases with the latitudinal difference $\Delta\theta$ between the spacecraft and the flare. Based on the delay of particle release time derived from in-ecliptic measurements relative to that from high-latitude measurements, we can conclude that such a delay is related to the poor connection between the source and spacecraft.

In order to use the VDA method more reasonably, many studies have been done to investigate the validity of the method. The following are their main conclusions. First, when the parallel mean-free path (MFP) is large enough ($\lambda_\parallel > 0.3$ AU), interplanetary scattering has only a small effect on the derived solar release time (Kallenrode & Wibberenz 1990; Lintunen & Vainio 2004; Diaz et al. 2011). Second, when the background level is below 0.01% of the peak intensity of the flux, the onset time of the SEP event can be determined quite accurately (Sáiz et al. 2005). In the above works, the interplanetary scattering and background-level effects on the release time have been studied in detail. In this paper, we study how different source models and perpendicular diffusion affect the onset time of the SEP and VDA results. In Section 2 we describe the SEP transport model. In Section 3 we show the simulation results. In Section 4 we discuss and summarize our results.

2. MODEL

We model the transport of SEPs following the previous research (e.g., Qin et al. 2006, 2013; Zhang et al. 2009; Dröge et al. 2010; He et al. 2011; Zuo et al. 2011, 2013; Wang et al. 2012, 2014). A three-dimensional focused transport equation is written as (Skilling 1971; Schlickeiser 2002; Qin et al. 2006; Zhang et al. 2009)

$$\begin{aligned}\frac{\partial f}{\partial t} &= \nabla\cdot(\boldsymbol{\kappa}_\perp\cdot\nabla f) - \left(v\mu\hat{\boldsymbol{b}} + \boldsymbol{V}^{\rm sw}\right)\cdot\nabla f + \frac{\partial}{\partial\mu}\left(D_{\mu\mu}\frac{\partial f}{\partial\mu}\right)\\ &+ p\left[\frac{1-\mu^2}{2}\left(\nabla\cdot\boldsymbol{V}^{\rm sw} - \hat{\boldsymbol{b}}\hat{\boldsymbol{b}}:\nabla\boldsymbol{V}^{\rm sw}\right) + \mu^2\hat{\boldsymbol{b}}\hat{\boldsymbol{b}}:\nabla\boldsymbol{V}^{\rm sw}\right]\frac{\partial f}{\partial p}\\ &- \frac{1-\mu^2}{2}\left[-\frac{v}{L} + \mu\left(\nabla\cdot\boldsymbol{V}^{\rm sw} - 3\hat{\boldsymbol{b}}\hat{\boldsymbol{b}}:\nabla\boldsymbol{V}^{\rm sw}\right)\right]\frac{\partial f}{\partial\mu},\end{aligned} \tag{1}$$

where $f(\boldsymbol{x}, \mu, p, t)$ is the gyrophase-averaged distribution function; $\boldsymbol{x}$ is the position in a nonrotating heliographic coordinate system; p, μ, and v are the momentum, particle pitch-angle cosine, and speed, respectively, in the solar wind frame; t is the time; $\boldsymbol{V}^{\rm sw} = V^{\rm sw}\hat{\boldsymbol{r}}$ is the solar wind velocity; $\hat{\boldsymbol{b}}$ is a unit vector along the local magnetic field; and L is the magnetic focusing length given by $L = (\hat{\boldsymbol{b}}\cdot\nabla ln B_0)^{-1}$ with B_0 being the magnitude of the background magnetic field. This equation includes many important particle transport effects, such as particle streaming along the field line, magnetic focusing in the diverging interplanetary magnetic field (IMF), adiabatic cooling in the expanding solar wind, and the diffusion coefficients parallel and perpendicular to the IMF. Here, we use the Parker field model for the IMF, and the solar wind speed is 400 km s^{-1}.

The relationship between $D_{\mu\mu}$ and parallel MFP $\lambda_\parallel$ is written as (Jokipii 1966; Hasselmann 1968; Earl 1974)

$$\lambda_\parallel = \frac{3v}{8}\int_{-1}^{+1}\frac{(1-\mu^2)^2}{D_{\mu\mu}}d\mu, \tag{2}$$

and the parallel diffusion coefficient $\kappa_\parallel$ can be written as $\kappa_\parallel = v\lambda_\parallel/3$.

We follow the model for the pitch-angle diffusion coefficient from Beeck & Wibberenz (1986), see also (Qin et al. 2005)

$$D_{\mu\mu} = D_0 v p^{q-2}\{|\mu|^{q-1} + h\}(1-\mu^2), \tag{3}$$

where the constant D_0 controls the magnetic field fluctuation level. The constant q is chosen as 5/3 for a Kolmogorov spectrum type of the power spectral density of magnetic field turbulence in the inertial range. Furthermore, $h = 0.01$ is chosen for the nonlinear effect of pitch-angle diffusion at $\mu = 0$ in the solar wind (Qin & Shalchi 2009, 2014).

The relation of the particle momentum and the perpendicular diffusion coefficient is set as

$$\boldsymbol{\kappa}_\perp = \kappa_0\left(\frac{p}{1\ \text{GeV}\ c^{-1}}\right)^{1/3}\left(\boldsymbol{I} - \hat{\boldsymbol{b}}\hat{\boldsymbol{b}}\right), \tag{4}$$

where p is the particle momentum. Different perpendicular diffusion coefficients could be obtained by altering κ_0, and $\kappa_\perp/\kappa_\parallel$ is set to 0.01 in the ecliptic at 1 AU in our simulations. Note that we use this formula for the purpose of simplicity. There are some more complete models that are developed to describe the particle diffusion in magnetic turbulence, such as the nonlinear guiding center theory (Matthaeus et al. 2003; Qin & Zhang 2014).

We use boundary values to model the particle injection from the source, which is chosen in the following form:

$$f_b(z \leqslant 0.05\ \text{AU}, E_k, \theta, \varphi, t) = a\frac{E_k^{-\gamma}}{p^2}\xi(t,\theta,\varphi), \tag{5}$$

$$\xi(t,\theta,\varphi) = \begin{cases} \frac{1}{t}\exp\left[-\frac{t_c}{t}\left(\frac{\phi_s}{\phi_0}\right)^2 - \frac{t}{t_l}\right]H(\phi_s - |\phi(\theta,\varphi)|) & \text{Case 1,}\\ \left\{\frac{1}{t}\exp\left[-\frac{t_c}{t}\left(\frac{\phi_s}{\phi_0}\right)^2 - \frac{t}{t_l}\right]H(\phi_s - |\phi(\theta,\varphi)|) + \frac{1}{t}\exp\left[-\frac{t_c}{t}\left(\frac{\phi(\theta,\varphi)}{\phi_0}\right)^2 - \frac{t}{t_l}\right][1 - H(\phi_s - |\phi(\theta,\varphi)|)]\right\} & \text{Case 2,}\\ \frac{1}{t}\exp\left(-\frac{t_c}{t} - \frac{t}{t_l}\right)\exp\left(-\frac{|\phi(\theta,\varphi)|}{\phi_0}\right)H(\phi_s - |\phi(\theta,\varphi)|) & \text{Case 3.}\end{cases}$$

Here the particles are injected from the SEP source near the Sun, and $\phi(\theta, \varphi)$ is the angle between the source center and any point (θ, φ) near the Sun where the particles are injected. We use three models to describe different scenarios. In case 1, SEPs are accelerated by a flare, and particles do not propagate in the solar atmosphere. In case 2, SEPs are accelerated by a flare, and particles can propagate in the solar atmosphere. In case 3, SEPs are accelerated by a coronal shock. The flare source model in case 1 and 2 is obtained by following Reid (1964), and the shock model in case 3 is obtained following Kallenrode & Wibberenz (1997). Here, $H(x)$ is the Heaviside step function; ϕ_s is used to control the angular width of the source; ϕ_0 describes how the source intensity decreases toward the flank of the source, and it is set to 15° in the following simulations unless otherwise stated

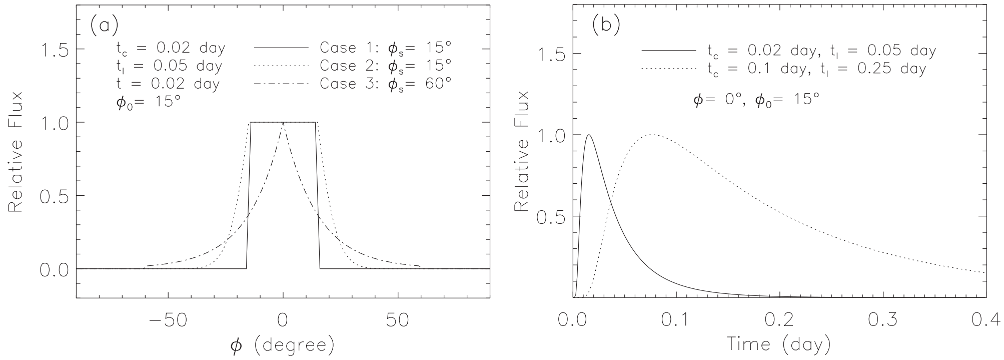

Figure 1. Comparison of proton fluxes with different source models and source durations.

in the text; E_k is the energy of the particles; γ is the spectral index of the source particles; and t_c and t_l are time constants to indicate the rise and decay timescales, respectively. Here, we set a typical value of $\gamma = 3$ for the spectral index of the source particles. Figure 1(a) shows spatial distributions of flux at $t = 0.02$ day normalized by the peaks in the cases of the different source models (cases 1–3). Here, the parameters of source duration are set to $t_c = 0.02$ day and $t_l = 0.05$ day, and ϕ_s is set to different values corresponding to different source models. Figure 1(b) shows time profiles of the flux at $\phi = 0^\circ$ normalized by the peaks in the cases of different source duration. In our simulations, the source rotates with the rotation of the Sun.

We use a time-backward Markov stochastic process method to solve the transport Equation (1) (Zhang 1999). The initial boundary value problem of the SEP transport equation can be reformulated into stochastic differential equations, so it can be solved by a Monte Carlo simulation of a Markov stochastic process, and the SEP distribution function can be derived. In this method, we trace particles from the observation point back to the injection time from the SEP source. Only those particles in the source region at the initial time contribute to the statistics. For a detailed description of this method, please refer to Qin et al. (2006).

3. RESULTS

Note that the inner boundary is 0.05 AU, and the outer boundary is 50 AU. We use two different parallel MFPs $\lambda_\parallel = 0.126$ AU and $\lambda_\parallel = 0.3$ AU for 10 MeV protons in the ecliptic at 1 AU. Based on the simulation results of Diaz et al. (2011), interplanetary scattering has a great effect on the derived solar release time of the VDA method in the case of $\lambda_\parallel = 0.126$ AU, and it has only a small effect on the derived solar release time in the case of $\lambda_\parallel = 0.3$ AU. As a result, $\lambda_\parallel = 0.126$ AU is used as strong scattering in the interplanetary space, and $\lambda_\parallel = 0.3$ AU is used as weak scattering. In the following simulations, $\lambda_\parallel$ is set to 0.126 AU for 10 MeV particles in the ecliptic at 1 AU, unless otherwise stated in the text. We choose different t_c and t_l to study different durations of the source. We set $t_c = 0.02$ day (0.48 hr) and $t_l = 0.05$ day (1.2 hr) as an impulsive duration and set $t_c = 0.1$ day (2.4 hr) and $t_l = 0.25$ day (6 hr) as a gradual duration case.

Before we can determine the detected onset time from the simulated time profiles, we have to define the background level of the flux. In a real SEP event, this background may be due either to the level of galactic cosmic rays or to a previous SEP event. In this paper, we choose the background level as a constant fraction A of the maximum intensity. In each energy channel, we set the background fraction A as 10^{-5}, 10^{-3}, and 10^{-1}, corresponding to a low background level, middle background level, and high background level, respectively.

3.1. *Particles Not Propagating in the Solar Atmosphere*

In this section, we use the source model as shown in case 1 of Equation (5), i.e., particles are accelerated by a flare without propagating in the solar atmosphere. In addition, ϕ_s is set to 15°.

3.1.1. *Effect of Perpendicular Diffusion on the Onset Time of an SEP Event*

Figure 2(a) shows time profiles of a 10 MeV proton omnidirectional flux in the cases with and without perpendicular diffusion. The source duration is set as a gradual one, i.e., $t_c = 0.1$ day and $t_l = 0.25$ day as a gradual duration. The solid line indicates the case with perpendicular diffusion, and the dash-dotted line indicates the case without perpendicular diffusion. The observer is located in the ecliptic at 1 AU and 0° longitude, and the observer's field line is connected directly to the center of the source near the Sun. Comparing the time profiles of the flux, we find that the observed flux is smaller with the perpendicular diffusion. The reason is that, in this situation, the particles can leave field lines because of perpendicular diffusion. Figure 2(b) shows the time profiles of the flux normalized by the peaks. As one can see, the onset times are much the same with and without perpendicular diffusion, so the two cases could not be distinguished observationally. We also show the normalized flux to study the onset time in the following cases.

3.1.2. *Observers at Different Locations*

Figure 3(a) shows time profiles of a 10 MeV proton omnidirectional flux detected by three observers. The source duration is set as a gradual one. The observers are located in the ecliptic with different longitudes such that the center of the source is located at 0°, 50° west, and 50° east of the foot-point of the observer, which are labeled as 0° (solid line), $W50^\circ$ (dash-dotted line), and $E50^\circ$ (dashed line), respectively. When an observer is connected to the center of the source directly by the IMF, energetic particles can arrive at the observers location by following the field lines. In the cases of $W50^\circ$ and $E50^\circ$, the two observers' field lines are disconnected from the SEP source because the half-width of the source is only 15°. Therefore, energetic particles can only be detected by the observers with the effect of perpendicular diffusion during the onset time. According to the above three observers, the peak of the flux is the largest when the observer is connected directly to the source by the IMF, and it is the smallest when the the center of the source is located at 50° west of the IMF foot-point of the observer. Because of

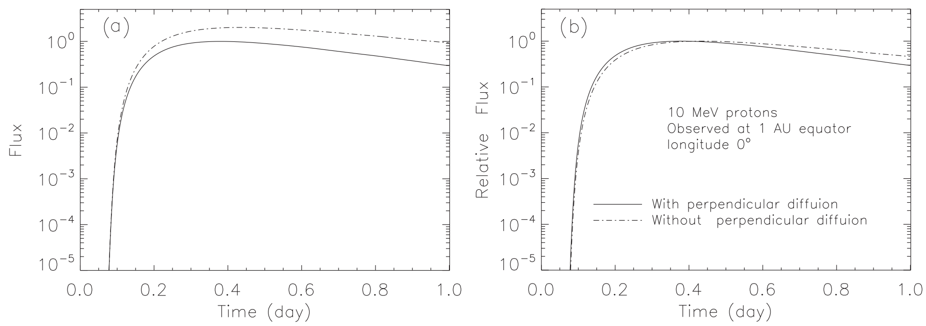

Figure 2. Comparison of 10 MeV proton fluxes with perpendicular diffusion (solid line) and without perpendicular diffusion (dash-dotted line).

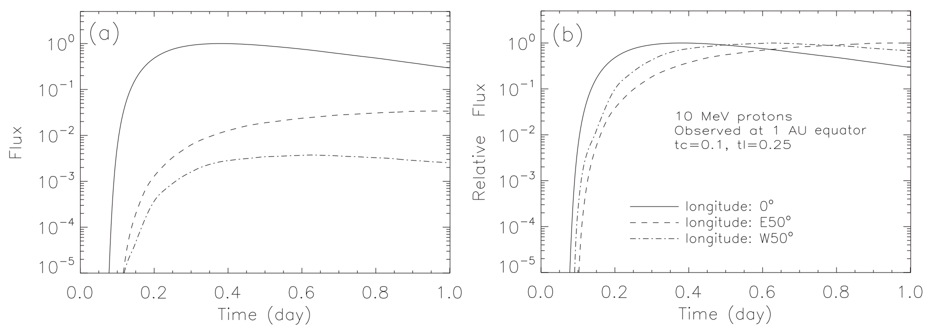

Figure 3. Comparison of 10 MeV proton fluxes observed at different locations.

the effect of convection, the particles rotate with the Sun after they are emitted. More particles are injected into the field line of the observer if the source is located at 50° east than that at 50° west. As a result, the flux of $W50^\circ$ is smaller than that of $E50^\circ$. This effect would lead to the eastwest asymmetry of the SEP distribution in the interplanetary space. Figure 3(b) shows time profiles of a normalized omnidirectional flux for the cases in Figure 3(a). According to the observers, the onset time is the earliest when the observer is connected to the source, and it is the latest when the center of the source is located at 50° east of the IMF foot-point of the observer.

3.2. Different Source and Transport Models

Figure 4 shows time profiles of the 10 MeV proton normalized omnidirectional flux in the cases with different source models. The solid line indicates that particles do not propagate in the solar atmosphere with case 1 of Equation (5) ($\phi_s = 15^\circ$). The dashed line indicates that particles can propagate in the solar atmosphere with case 2 of Equation (5) ($\phi_s = 15^\circ$). The dash-dotted line indicates that particles are accelerated by a coronal shock with case 3 of Equation (5) ($\phi_s = 60^\circ$). In all three cases, the observer is located in the ecliptic at 1 AU and is connected to the center of the source. The time profiles are similar during the rising phase in all cases. As a result, when the observer is connected to the center of the source, the spatial distribution of the source does not affect the VDA results.

Figure 5 shows time profiles of a 10 MeV proton omnidirectional flux in the cases with different propagation models. In all cases, the observer is located in the ecliptic at 1 AU, and the center of the SEP source is E50° to the observer with $\phi_s = 15^\circ$. The source parameter ϕ_0 is set to 15° and 5° in Figures 5(a) and (b), respectively. The source model of the solid lines and dashed lines is in case 2 of Equation (5). The source model of the dash-dotted line is in case 1 of Equation (5), which indicates that particles do not propagate in the solar atmosphere. In addition, the solid and dash-dotted lines indicate that particles propagate in the interplanetary space with perpendicular diffusion, and the dashed lines indicate particles without perpendicular diffusion. In Figure 5(a), the flux indicated by the solid line is the largest, and that indicated by the dash-dotted line is the smallest. In Figure 5(b), the flux indicated by the solid line is the largest, and that indicated by the dashed line is the smallest. Therefore, the propagation effect of particles in the solar atmosphere is stronger/weaker than that of the perpendicular diffusion in the interplanetary space when the particle source decreases slower/faster toward the flank of the source with $\phi_0 = 15^\circ/\phi_0 = 5^\circ$. Comparing these two panels, the timescale of the rising phase of the flux, indicated by a solid line in panel (a), is smaller than that in panel (b).

3.3. Particles Propagating in the Solar Atmosphere

Figure 6(a) shows time profiles of a 10 MeV proton omnidirectional flux observed at different locations, and Figure 6(b) shows the normalized fluxes. We use the source model as shown in case 2 of Equation (5), and $\lambda_\parallel$ is set to 0.126 AU for 10 MeV particles at the 1 AU equatorial plane. Here, particles produced by a flare can propagate in the solar atmosphere, and they can also cross field lines with perpendicular diffusion in the interplanetary space. The source parameter ϕ_s is set to 15°. Three observers are located in the ecliptic at 1 AU with different longitudes such that the center of the source is located at 0°, $W50^\circ$, and $E50^\circ$, respectively, to the foot-point of the observer. According to the observers, the flux is the largest when the observer is connected to the center of the source, and it is the smallest when the center of the source is located at $W50^\circ$ to the foot-point of the observer. Figure 6(b) reveals that the onset times of the three fluxes are different. In the source model, when ϕ is larger than 15°, the time profile of the SEP source changes with ϕ. As a result, the time profiles of the SEP flux in the cases of $E50^\circ$ and $W50^\circ$ increase more slowly than that in the case of longitude 0°. In this condition, when the observer is far from the center

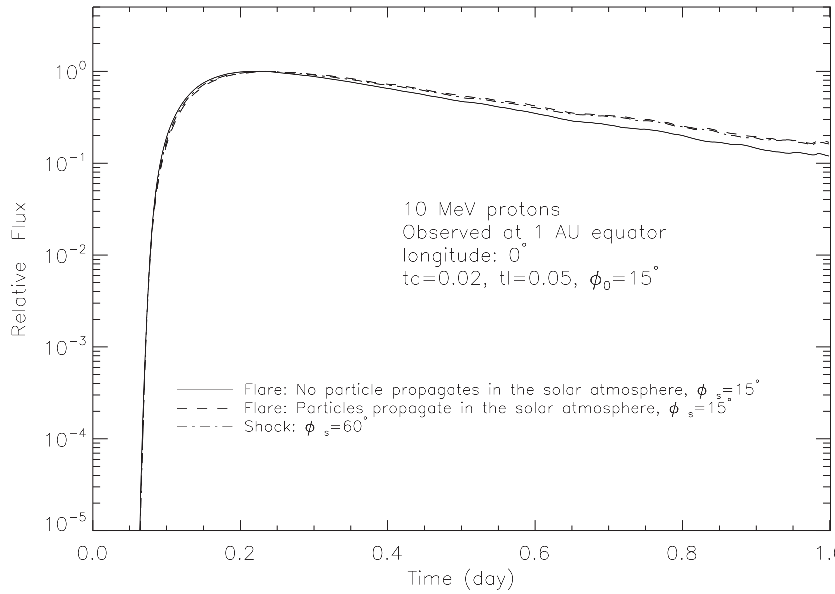

Figure 4. Comparison of 10 MeV proton fluxes observed at 1 AU that are produced by different SEP sources. The solid line indicates the case when particles are accelerated by a flare, and particles do not propagate in the solar atmosphere. The dashed line indicates the case when particles are accelerated by a flare, and particles can propagate in the solar atmosphere. The dash-dotted line indicates the case when particles are accelerated by a coronal shock.

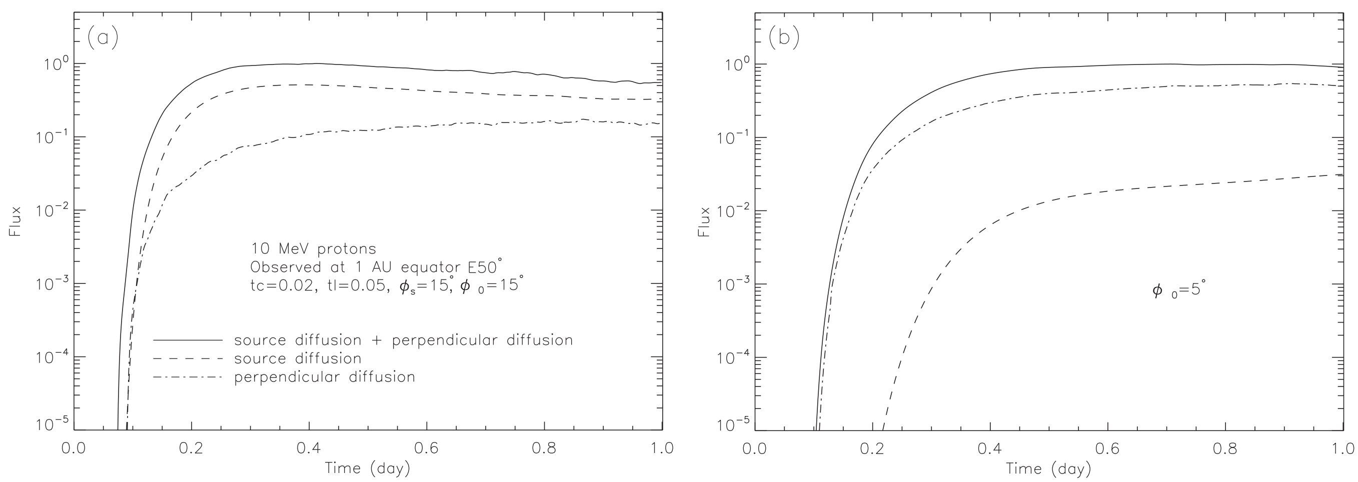

Figure 5. Comparison of 10 MeV proton fluxes in the cases with different propagation models. The solid lines indicate the case when particles can propagate in the solar atmosphere and can also cross the field lines in the interplanetary space with perpendicular diffusion. The dashed lines indicate the case when particles can propagate in the solar atmosphere, but without perpendicular diffusion in the interplanetary space. The dash-dotted lines indicate the case when particles can cross the field lines in the interplanetary space with perpendicular diffusion, but without propagation in the solar atmosphere.

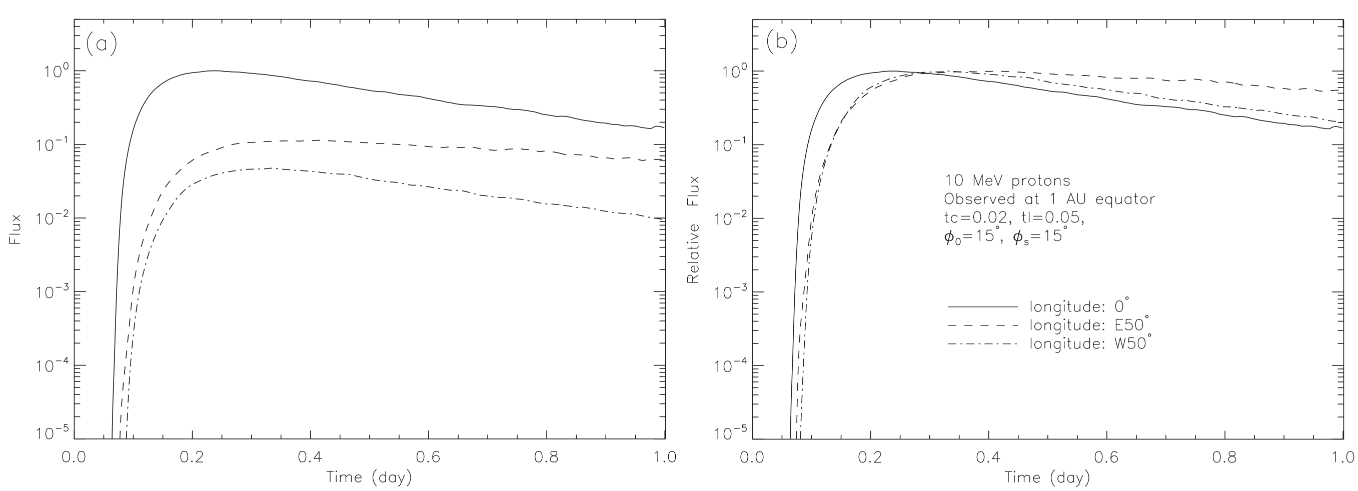

Figure 6. Comparison of 10 MeV proton fluxes observed at different locations. The particles are accelerated by a flare, and the ϕ_s is set to 15°.

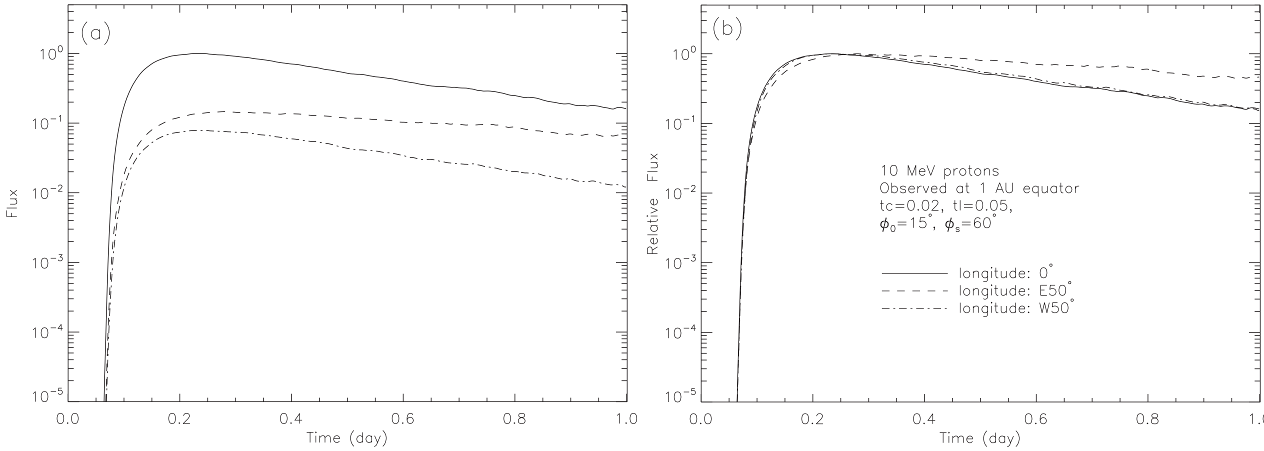

Figure 7. Comparison of 10 MeV proton fluxes observed at different locations. The particles are accelerated by a coronal shock, and the ϕ_s is set to 60°.

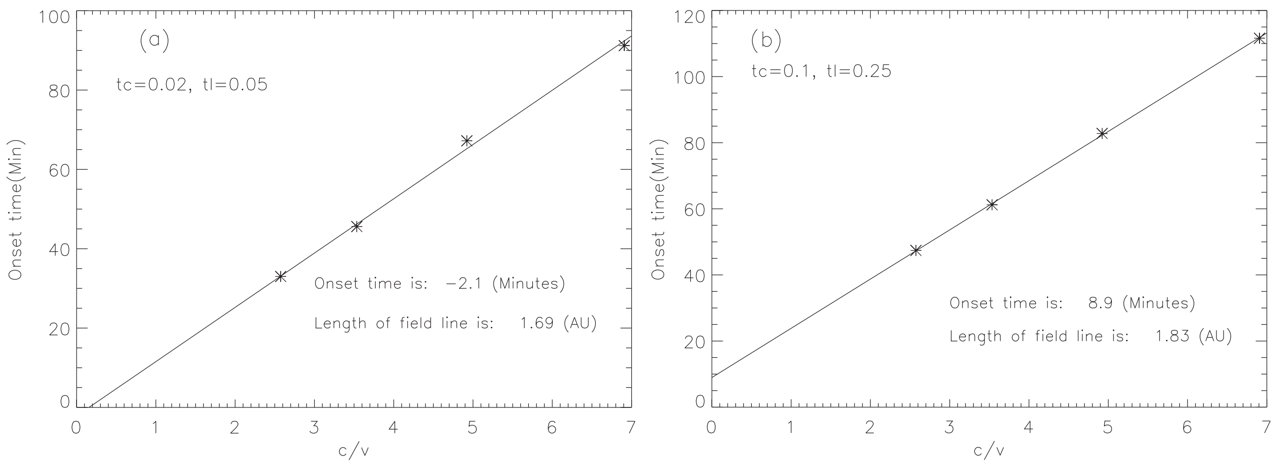

Figure 8. Results of the SEP release time and path length derived from the VDA method.

of the source ($\phi > 15°$), the angular distance should affect the VDA results.

3.4. Particles Accelerated by a Large Corona Shock

Figure 7 is similar to Figure 6 but with a different SEP source near the Sun. We use the SEP source model as shown in case 3 of Equation (5), and $\lambda_\parallel$ is set to 0.126 AU for 10 MeV particles at the 1 AU equatorial plane. Particles are accelerated by a corona shock, and they can also cross the field lines with perpendicular diffusion in the interplanetary space. The source parameter ϕ_s is set to 60°, and ϕ_0 is set to 15°. Three observers are located at the 1 AU equatorial plane with different longitudes such that the center of the source is located at 0°, $W50°$, and $E50°$, respectively, to the foot-point of the observer. In this case, the observers are connected to the source by magnetic field lines. Therefore, the effects of particles propagating in the solar atmosphere and perpendicular diffusion in the interplanetary space have little effect on the onset time of SEP fluxes. Because the time profile of the source does not change with ϕ in our model, the time profiles of fluxes detected by three observers are similar during the rising phase in Figure 7(b). As a result, the angular distance between the center of the source and the observer should not affect the VDA results. However, if the time profile of the SEP source changes with angular distance, the time profiles of flux detected by the observers should be different. This conclusion could be deduced from the results in Figure 6. In this case, the VDA results should change with the angular distance between the center of source and observer.

3.5. VDA Method Results

In this subsection, we will study how the perpendicular diffusion and different source models affect the VDA method results. The VDA method assumes that the first observed particles are the ones traveling along the magnetic field lines, and the path length traveled by the particles is independent of energy. If this holds, the transport time for SEPs is given by

$$t_o - t_i = \frac{L}{v}, \tag{6}$$

where L is a constant that represents the field line length, t_o is the onset time of the SEP flux that depends on particle speed, t_i is a constant that represents the release time of particles on the source, and v is the speed of the energetic particles.

Figures 8(a) and (b) show the dispersion of the onset time changes with c/v according to different source durations, where the observers are located at equator 0° longitude and the observer's field line is connected directly to the center of the source near the Sun. The only difference between Figures 8(a) and (b) is the source duration times. In Figure 8, the source model is set as case 1 of Equation (5), and the source parameter ϕ_s is set to 15°. Here, we get time profiles of SEP fluxes with simulations for four energy channels: 10 MeV, 20 MeV, 40 MeV,

Table 1
Results of VDA Method with Strong Scattering[a]

Case	Duration	Background	Location	t_i (minutes)	L (AU)
			Center	−2.1	1.69
1	Impulsive	Low	$W50^\circ$	−12	2.42
			$E50^\circ$	−18	2.51
			Center	−1.7	1.86
2	Impulsive	Middle	$W50^\circ$	−8.3	2.38
			$E50^\circ$	−18	2.68
			Center	−0.98	2.34
3	Impulsive	High	$W50^\circ$	−23	3.95
			$E50^\circ$	−43	4.83
			Center	8.9	1.83
4	Gradual	Low	$W50^\circ$	1.5	2.39
			$E50^\circ$	−8.9	2.70
			Center	12	2.09
5	Gradual	Middle	$W50^\circ$	9.9	2.66
			$E50^\circ$	−7.7	3.34
			Center	26	2.98
6	Gradual	High	$W50^\circ$	26	4.65
			$E50^\circ$	−6.9	6.45

Note. [a] In this table, $\lambda_\parallel$ is set to 0.126 AU for 10 MeV protons in the ecliptic at 1 AU.

Table 2
Results of VDA Method with Weak Scattering[a]

Case	Duration	Background	Location	t_i (minutes)	L (AU)
			Center	2.8	1.34
1	Impulsive	Low	$W50^\circ$	−1.3	1.60
			$E50^\circ$	2.1	1.39
			Center	2.6	1.46
2	Impulsive	Middle	$W50^\circ$	6.1	1.52
			$E50^\circ$	4.0	1.41
			Center	6.8	1.70
3	Impulsive	High	$W50^\circ$	6.9	1.87
			$E50^\circ$	6.0	1.84
			Center	11	1.48
4	Gradual	Low	$W50^\circ$	13	1.57
			$E50^\circ$	14	1.43
			Center	16	1.61
5	Gradual	Middle	$W50^\circ$	17	1.78
			$E50^\circ$	20	1.63
			Center	38	1.90
6	Gradual	High	$W50^\circ$	44	2.16
			$E50^\circ$	42	2.67

Note. [a] In this table, $\lambda_\parallel$ is set to 0.3 AU for 10 MeV protons in the ecliptic at 1 AU.

and 80 MeV. We set the SEP background as 10^{-5} of the flux peak, indicating a low background. From the SEP fluxes we obtain the onset times as the the times when the fluxes rise above the background. As one can see, the onset time increases linearly with c/v. Based on the results of data fitting, the release time near the Sun and the interplanetary field length can be derived.

With different observing locations, background levels, and source duration times, the calculated source release times and path lengths from the VDA method with simulation data are listed in Table 1. In our simulations, the source release time is set to 0, and the IMF is set to the Parker field model with the solar wind speed 400 km s^{-1}. In this table, the source release time and path length derived from VDA are labeled as t_i and L, respectively. Also, $\lambda_\parallel$ is set to 0.126 AU for 10 MeV protons in the ecliptic at 1 AU. The source model is set as case 1 of Equation (5), and ϕ_s is set to 15°. The observers are all located at the 1 AU equatorial plane but at different longitudes. When the observer is connected to the source, we have the following findings. In the cases of impulsive source duration (cases 1–3), the VDA release times are very close to the injection times on the source (less than three minutes). In the cases of gradual source duration (cases 4–6), however, the VDA release times are much later than the real release times. On the other hand, when the observer is disconnected from the source, the onset time of the SEP flux is later than the case when the observer is connected to the source. Therefore, the VDA results are generally much worse when the observer is disconnected from the source, with some exceptions. For example, in $W50^\circ$ of case 4, the release time of the VDA result is very close to the injection time on the source (less than two minutes). Obviously, this result is obtained fortuitously, and it cannot be taken as an indication that the VDA method is valid. In all six cases (cases 1–6), the path lengths obtained from the VDA method are longer than the real ones from the Parker spiral. Even when the observer is connected to the center of the flare with an impulsive duration source and a low background SEP level, the path length is still larger than that of the Parker spiral. This is because scattering in the interplanetary space could not be ignored because of the value of the MFP used in our simulation. Besides scattering in the interplanetary space, the source duration, source location, and SEP background level also affect the path length result of the VDA. Therefore, in case 6 of Table 1, the path lengths are much larger than that of the Parker spiral.

Table 2 is similar to Table 1 except for the MFP. Here, $\lambda_\parallel$ is set to 0.3 AU for 10 MeV protons in the ecliptic at 1 AU in Table 2. When the observer is connected to the source, we have the following findings. In cases 1 and 2, the VDA release times are very close to the injection times on the source (less than 3 minutes). However, in case 3 the difference between the VDA release time and the injection times can be as large as 6.8 minutes. In the cases of gradual source duration (cases 4–6), the VDA release times are much later than the real release times. Because of the larger MFPs, the path length derived from VDA in case 1 is much smaller than that in Table 1. The value of 1.34 AU is closer to the length of the Parker spiral. On the other hand, when the observer is disconnected from the source, the VDA release times are also very close to the injection times (less than three minutes) in case 1. However, in other cases, the VDA release times are generally worse when the observer is disconnected from the source, with some exceptions. In all six cases (cases 1–6), the path lengths obtained from the VDA method are longer than the real ones from the Parker spiral. Comparing Table 2 with Table 1, the path lengths obtained from the VDA method in Table 2 are smaller than that in Table 1.

Table 3 is similar to Table 1, except for the source model and MFP. In Table 3, the source model is set as case 2 of Equation (5), and particles can diffuse at the source region. The source parameters are set to $\phi_s = 15^\circ$, $t_c = 0.02$ day, and $t_l = 0.05$ day in all six cases. When $\lambda_\parallel$ is set to 0.126 AU for 10 MeV protons in the ecliptic at 1 AU, the propagation effect of particles in the solar atmosphere is stronger than that of the perpendicular diffusion in the interplanetary space. In cases 1–3, $\lambda_\parallel$ is set to 0.126 AU for 10 MeV protons, and $\lambda_\parallel$ is set to 0.3 AU for 10 MeV protons in cases 4–6. Comparing cases 1–3 in Table 3 with the impulsive duration cases in Table 1, we have the following findings. The VDA release times are much closer to the injection times on the source in Table 3 than that in Table 1,

Table 3
The Effects of Source Diffusion in the VDA Method

Case	Scattering	Background	Location	t_i (minutes)	L (AU)
			Center	−2.1	1.69
1	Strong[a]	Low	$W50°$	−0.91	1.91
			$E50°$	−4.8	1.96
			Center	0.41	1.82
2	Strong[a]	Middle	$W50°$	−6.9	2.41
			$E50°$	−5.9	2.31
			Center	−0.88	2.38
3	Strong[a]	High	$W50°$	2.8	3.29
			$E50°$	−0.72	3.34
			Center	2.8	1.34
4	Weak[b]	Low	$W50°$	0.4	1.56
			$E50°$	2.1	1.39
			Center	3.5	1.45
5	Weak[b]	Middle	$W50°$	4.6	1.63
			$E50°$	3.9	1.51
			Center	8.3	1.69
6	Weak[b]	High	$W50°$	11	2.02
			$E50°$	11	1.91

Notes.
[a] $\lambda_\parallel$ is set to 0.126 AU for 10 MeV protons in the ecliptic at 1 AU.
[b] $\lambda_\parallel$ is set to 0.3 AU for 10 MeV protons in the ecliptic at 1 AU.

and the path lengths in Table 3 are generally smaller than that in Table 1. The difference between the VDA release times and the injection times are within seven minutes. Comparing cases 4–6 in Table 3 with the impulsive duration cases in Table 2, we find that the VDA results are similar in these two tables, especially in the low-background case. This is because when $\lambda_\parallel$ is set to 0.3 AU for 10 MeV protons at the 1 AU equatorial plane, the effect of perpendicular diffusion in the interplanetary space is stronger than that of particles propagating in the solar atmosphere.

4. DISCUSSION AND CONCLUSIONS

In this paper, we discuss the uncertainty of the simple assumptions of the VDA method. First, the VDA results could be significantly affected by interplanetary scattering (Kallenrode & Wibberenz 1990; Lintunen & Vainio 2004; Diaz et al. 2011). Second, the onset time of the SEP event is hard to determine in practical applications because it can be significantly delayed by the background level (Sáiz et al. 2005). Third, particles can cross the field lines when they transport in the space. The perpendicular diffusion plays a very important role in the release time determination, especially when the observer's field line is disconnected from the source (Zhang et al. 2009; Qin et al. 2011; He et al. 2011). Fourth, different source models affect the accuracy of results of the VDA method. For example, particles accelerated by a flare may directly propagate in the solar atmosphere (Wibberenz et al. 1989), and a large shock could provide a very wide source (Mason et al. 1984; Gosling 1993; Zank et al. 2000; Li et al. 2003).

By numerically solving the focused Fokker–Planck equation, we have calculated SEP intensity time profiles, including the perpendicular diffusion. We set different source durations and background levels to study the onset times observed by observers. Comparing the time profiles of SEP fluxes observed at different locations, we have studied the effect of different source models and perpendicular diffusion on the onset times of SEP events and its influence on the VDA method results. Our new findings are as follows.

1. If SEPs are produced by a solar flare, they can spread much wider than the source region by two possible mechanisms. In the first one, particles propagate in the solar atmosphere. In the second one, particles cross the field lines in the interplanetary space by perpendicular diffusion. In this case, the VDA results can be affected by the above two mechanisms when the observer is not connected to the source at the initial time. In addition, because of the effect of convection, more particles are injected in the field line of the observer when the source is located at the east flank to the foot-point of the observer than that in the case of the west flank. This effect would lead to the eastwest asymmetry of the SEP distribution in the interplanetary space.
2. When the observer is connected to the source by the IMF, comparing the time profiles of fluxes in the cases with and without perpendicular diffusion, or with and without particle propagation in the solar atmosphere, the onset times are much the same. In this case, the effects of the particles perpendicular diffusion in the interplanetary space and propagation in the solar atmosphere do not affect the results of the VDA significantly. The results obtained by previous simulations, which did not include these two mechanisms (Kallenrode & Wibberenz 1990; Lintunen & Vainio 2004; Sáiz et al. 2005; Diaz et al. 2011), still holds when these two mechanisms are included.
3. If SEPs accelerated by a solar flare cannot propagate in the solar atmosphere, the SEP source region is about the size of the solar flare. In this case, when the observer is disconnected from the source by the IMF, the energetic particles can be detected with the effect of the perpendicular diffusion. The onset time is later when the observer is disconnected from the source than when the observer is connected to the source. In the cases of weak scattering, the solar release time derived from the VDA method is close to the injection time when the observer is disconnected from the source with impulsive source duration and low background. However, in the cases of strong scattering, the release time and the path length obtained from the VDA method are much different from the real values, except in some fortuitous cases.
4. If SEPs accelerated by a solar flare can propagate in the solar atmosphere, the SEP source region should be larger than the size of the solar flare as time goes by. When the observer is far from the SEP source at the initial time, the particles will spend some time on leaving the source to the observer's field line. As a result, the timescale of the rising phase of the flux is larger than that in the case when the observer is connected to the center of the source. When source diffusion in the solar atmosphere is faster than perpendicular diffusion in the interplanetary space, the solar release time derived from the VDA method is close to the injection time when the observer is disconnected from the source with a low background. If source diffusion in the solar atmosphere is slower than perpendicular diffusion, the VDA results are significantly affected by the MFP. In the case of weak scattering, the solar release time derived from the VDA method is still valid with impulsive source duration and low background. However, in the case of strong scattering, the solar release time derived from the VDA method is not valid.

5. If SEPs are accelerated by a large-scale corona shock, the source can cover a very wide region because of the size of the corona shock. The observers located at different locations can be connected to the Sun simultaneously. Therefore, the effects of particles propagating in the solar atmosphere and perpendicular diffusion in the interplanetary space have little effect on the onset time of SEP fluxes and the VDA results, and the accuracy of the VDA method depends on other conditions. If the time profile of the SEP source does not change with the angular distance between the foot-point of the observer's magnetic field line and the center of the source, the onset time of fluxes observed at different locations could be much the same. In this case, the VDA results do not change with the angular distance. Otherwise, the time profile of the SEP source changes with angular distance, and the onset time of the SEP flux and the VDA results will change with angular distance.
6. In our simulations, the VDA results could be significantly affected by the location and size of the SEP source. As shown in previous studies (Kallenrode & Wibberenz 1990; Lintunen & Vainio 2004; Sáiz et al. 2005; Diaz et al. 2011), the VDA results are also significantly affected by the time profile of the source, the parallel MFP, and the background level. In order to reduce error in the results of the VDA method, an ideal SEP event should meet the following conditions: impulsive source duration, large parallel MFP, low background level, and good connection between the observer and the source.

The authors thank the anonymous referee for valuable comments. We are partly supported by grants NNSFC 41374177, NNSFC 41125016, and NNSFC 41304135, the CMA grant GYHY201106011, and the Specialized Research Fund for State Key Laboratories of China. The computations were performed by the Numerical Forecast Modeling R&D and VR System of the State Key Laboratory of Space Weather and the Special HPC work stand of the Chinese Meridian Project.

REFERENCES

Beeck, J., & Wibberenz, G. 1986, ApJ, 311, 437
Dalla, S., Balogh, A., Krucker, S., et al. 2003a, AnGeo, 21, 1367
Dalla, S., Balogh, A., Krucker, S., et al. 2003b, GeoRL, 30, 8035
Diaz, I., Zhang, M., Qin, G., & Rassoul, H. K. 2011, ICRC, 10, 40
Ding, L.-G., Li, G., Jiang, Y., et al. 2014, ApJL, 793, L35
Dresing, N., Gómez-Herrero, R., Heber, B., et al. 2014, A&A, 567, A27
Dresing, N., Gómez-Herrero, R., Klassen, A., et al. 2012, SoPh, 281, 281
Dröge, W., Kartavykh, Y. Y., Klecker, B., & Kovaltsov, G. A. 2010, ApJ, 709, 912
Earl, J. 1974, ApJ, 193, 231
Forbush, S. E. 1946, PhRv, 70, 771
Gosling, J. T. 1993, JGR, 98, 18937
Hasselmann, K. 1968, ZGeo, 34, 353
He, H.-Q., Qin, G., & Zhang, M. 2011, ApJ, 734, 74
Huttunen-Heikinmaa, K., Valtonen, E., & Laitinen, T. 2005, A&A, 442, 673
Jokipii, J. R. 1966, ApJ, 146, 480
Kahler, S., & Ragot, B. R. 2006, ApJ, 646, 634
Kallenrode, M., & Wibberenz, G. 1997, JGR, 102, 22311
Kallenrode, M.-B., & Wibberenz, G. 1990, ICRC, 5, 229
Krucker, S., Larson, D. E., Lin, R. P., & Thompson, B. J. 1999, ApJ, 519, 864
Krucker, S., & Lin, R. P. 2000, ApJL, 542, L61
Li, C., Firoz, K. A., Sun, L., & Miroshnichenko, L. 2013, ApJ, 770, 34
Li, G., Zank, G., & Rice, W. 2003, JGRA, 108, 1082
Lintunen, J., & Vainio, R. 2004, A&A, 420, 343
Ma Sung, L. S., & Earl, J. A. 1978, ApJ, 222, 1080
Mason, G., Gloeckler, G., & Hovestadt, D. 1984, ApJ, 280, 902
Matthaeus, W. H., Qin, G., Bieber, J. W., & Zank, G. P. 2003, ApJL, 590, L53
McKibben, R. B. 1972, JGR, 77, 3957
Qin, G., He, H.-Q., & Zhang, M. 2011, ApJ, 738, 28
Qin, G., & Shalchi, A. 2009, ApJ, 707, 61
Qin, G., & Shalchi, A. 2014, PhPl, 21, 042906
Qin, G., Wang, Y., Zhang, M., & Dalla, S. 2013, ApJ, 766, 74
Qin, G., & Zhang, L.-H. 2014, ApJ, 787, 12
Qin, G., Zhang, M., Dwyer, J., Rassoul, H., & Mason, G. 2005, ApJ, 627, 562
Qin, G., Zhang, M., & Dwyer, J. R. 2006, JGRA, 111, 8101
Reames, D. V. 1999, SSRv, 90, 413
Reames, D. V. 2009, ApJ, 706, 844
Reames, D. V. 2013, SSRv, 175, 53
Reid, G. C. 1964, JGR, 69, 2659
Sáiz, A., Evenson, P., Ruffolo, D., & Bieber, J. W. 2005, ApJ, 626, 1131
Schlickeiser, R. 2002, Cosmic Ray Astrophysics (Berlin: Springer)
Skilling, J. 1971, ApJ, 170, 265
Tan, L. C., Malandraki, O. E., Reames, D. V., et al. 2012, ApJ, 750, 146
Van Hollebeke, M., Sung, L. M., & McDonald, F. 1975, SoPh, 41, 189
Wang, Y., Qin, G., & Zhang, M. 2012, ApJ, 752, 37
Wang, Y., Qin, G., Zhang, M., & Dalla, S. 2014, ApJ, 789, 157
Wibberenz, G., Kecskemety, K., Kunow, H., et al. 1989, SoPh, 124, 353
Zank, G. P., Rice, W. K. M., & Wu, C. C. 2000, JGR, 105, 25079
Zhang, M. 1999, ApJ, 513, 409
Zhang, M., McKibben, R. B., Lopate, C., et al. 2003, JGRA, 108, 1154
Zhang, M., Qin, G., & Rassoul, H. 2009, ApJ, 692, 109
Zuo, P., Zhang, M., Gamayunov, K., Rassoul, H., & Luo, X. 2011, ApJ, 738, 168
Zuo, P., Zhang, M., & Rassoul, H. K. 2013, ApJ, 767, 6